Received: 29 August 2022 | Revised: 5 October 2022 | Accepted: 11 October 2022

DOI: 10.1002/poc.4455

RESEARCH ARTICLE

Journal of Physical Organic Chemistry WILEY

Azaboracyclooctatetraenes reveal that the different aspects of triplet state Baird-aromaticity are nothing but different

Preethanuj Preethalayam[1] | **Nathalie Proos Vedin**[1] | **Slavko Radenković**[2] | **Henrik Ottosson**[1]

[1]Department of Chemistry – Ångström Laboratory, Uppsala University, Uppsala, Sweden

[2]Faculty of Science, University of Kragujevac, Kragujevac, Serbia

Correspondence
Henrik Ottosson, Department of Chemistry – Ångström Laboratory, Uppsala University, Box 523, 751 20 Uppsala, Sweden.
Email: henrik.ottosson@kemi.uu.se

Funding information
Serbian Ministry of Education, Science and Technological Development, Grant/Award Number: 451-03-68/2022-14/200122; Vetenskapsrådet, Grant/Award Number: 2019-05618; Wenner-Gren Foundation, Grant/Award Number: UPD 2020-0270

Abstract

The Baird-aromaticity of BN/CC cyclooctatetraene isosteres (azaboracyclooctatetraenes) in their lowest triplet states (T_1) has been explored through computations of various aromaticity indices that describe the different aspects of aromaticity (magnetic, electronic, energetic and geometric). While cyclooctatetraene (**COT**) is aromatic in its T_1 state following Baird's 4*n* rule, we now reveal that the degrees of Baird-aromaticity of its BN/CC isosteres vary with aromaticity aspect considered. The thermodynamically most stable octagonal $B_4N_4H_8$ isomer, having an alternating B and N pattern (borazocine, **B_4N_4COT-A**), is only weakly aromatic or nonaromatic in T_1 according to energetic and electronic indices, while magnetic descriptors suggest it to have about two thirds the Baird-aromaticity of T_1 state **COT** (**^{3}COT**). The extent of Baird-aromaticity of intermediate BN/CC isosteres also varies markedly with aromaticity aspect considered. The strong aromaticity of **$^3B_4N_4$COT-A** according to magnetic descriptors can be linked to the symmetries of the orbitals involved in the virtual transitions from occupied to unoccupied orbitals, which describe the response of a molecule in an external magnetic field. However, the magnetic aspect of T_1 state Baird-aromaticity (response aromaticity) is not related to the electronic and energetic aspects (intrinsic aromaticity), findings that underline earlier observations on differences between the various aspects of the aromaticity phenomenon (or phenomena).

KEYWORDS

aromaticity indices, Baird aromaticity, BN/CC isosterism, borazocine, heterocycles

1 | INTRODUCTION

Borazine, $B_3N_3H_6$, is a heteroaromatic molecule sometimes labeled as "inorganic benzene" (Chart 1),[1–4] although its extent of Hückel-aromaticity in the S_0 state has been debated for several decades.[5–15] When based on magnetic aromaticity indicators, it is found to be much less aromatic than benzene.[5,6,9–12] Yet, features of the magnetically induced current densities of the two molecules (a diatropic ring current in benzene while local circulations at the N atoms in borazine) can be related via a set of intermediate current densities computed for

model molecules with non-integer nuclear charges in between those of C, B and N.[10] Furthermore, a recent analysis of the experimental electron density reveals an island-like electron delocalization at the N atoms, leading to only weak aromatic character,[13] in line with conclusions based on computed electronic indices.[11,14,15] Interestingly, the index of deviation from aromaticity (IDA), which measures the degree of electron density polarization, estimated borazine in S_0 to be even antiaromatic.[11] In contrast, geometric and energetic indices suggest that it still exhibits a degree of aromaticity.[7,8,12] Now, in the lowest ππ* triplet state (T_1) [4*n*]annulenes are normally aromatic according to Baird's 4*n* rule.[16–21] Herein we explore if azabora[4*n*]annulenes in their T_1 states also exhibit extensive variations with regard to their potential Baird-aromaticity when evaluated based on the different aromaticity aspects.

The smallest member, 1,3,2,4-diazadiboretidine (Chart 1), first synthesized in the 1960s,[22–24] exhibits no T_1 state Baird-aromatic character, although it was noted that a D_{2h} symmetric transition state structure has a negative NICS value and a diatropic ring current (electronic indices, in contrast, suggested a nonaromatic character of this structure).[25] Yet, as **CBD** in its T_1 state has a moderate Baird-aromaticity[26–28] one may assume that 1,3,2,4-diazadiboretidine is not an ideal molecule for a test on Baird-aromaticity of azabora[4*n*]annulenes in their T_1 states. If one considers the all-carbon [4*n*]annulenes, it has been observed based on NICS and isomerization stabilization energies (ISE) that cyclooctatetraene in its T_1 state (^{3}**COT**) exhibits a more substantial Baird-aromaticity.[29–31] Hence, we argue that borazocine (Chart 1), octahydro-1,3,5,7,2,4,6,8-tetraazatetraborocine (**B_4N_4COT-A**), also first synthesized in the 1960s,[24,32,33] is a more suitable scaffold for exploration of the potential Baird-aromaticity in azabora[4*n*]annulenes. The potential Hückel antiaromaticity of **B_4N_4COT-A** in S_0 and the aromaticity of the dianion have earlier been explored computationally,[34,35] and the results for the S_0 state dianion are noteworthy as they can be related to the T_1 state of the neutral species. Indeed, based on valence bond (VB) theory ^{3}**B_4N_4COT-A** could be more Baird-aromatic than borazine is Hückel-aromatic in S_0 because the T_1 state of **B_4N_4COT-A** requires structures with two atoms with one unpaired same-spin π-electron each (Figure 1). This requires transfer of an electron from an N atom to a B atom, and that VB-structures such as **I** - **III** make significant contributions while structures such as **IV** - **VI** contribute much less (Figure 1B). However, as becomes clear through our study, the extent of Baird-aromaticity varies extensively with aromaticity aspect considered.

Interestingly, large differences between the magnetic and energetic aromaticity aspects have earlier been observed for the 10π-electron systems $(N_6H_6)^{2+}$ and $C_2N_4H_6$ as these were about as aromatic as benzene

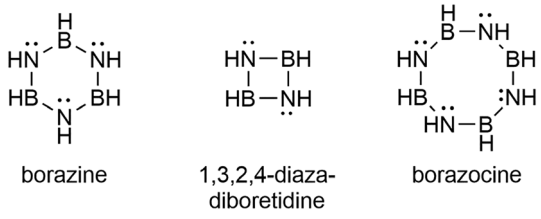

CHART 1 The BN/CC isosteres of benzene, cyclobutadiene and cyclooctatetraene.

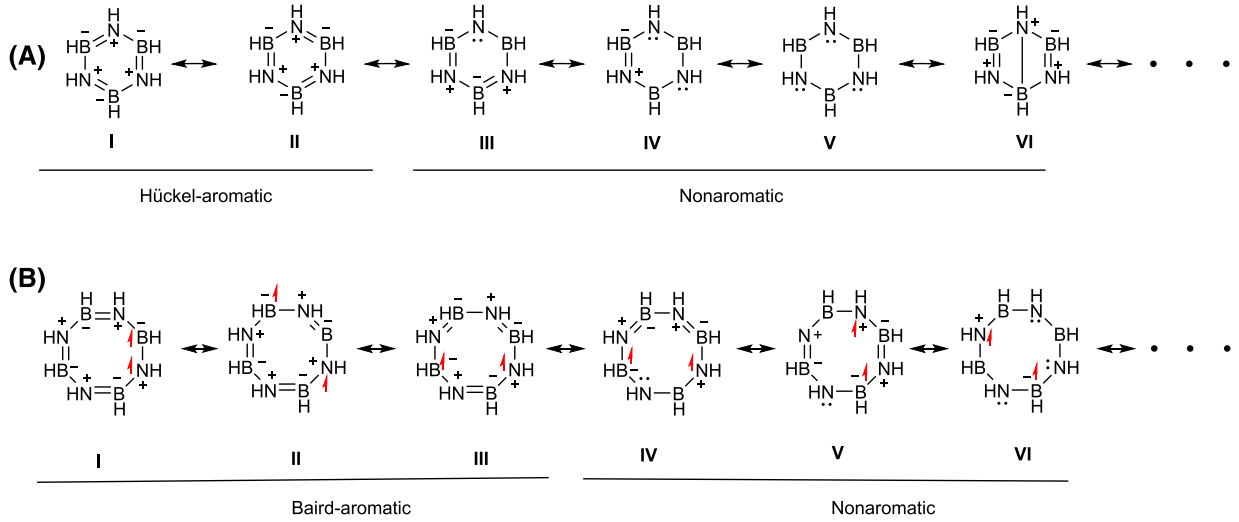

FIGURE 1 Various resonance structures of (A) borazine in S_0, and (B) borazocine in T_1, showing their potential Hückel- and Baird-aromatic character.

according to magnetic criteria but much less when based on electronic ones.[36] It was concluded that "*[a]romatic compounds exhibit ring current induced magnetic shielding, but the reverse conclusion that ring current induced magnetic shielding identifies aromaticity is not justified.*"[36] Indeed, it has been shown mathematically that there is no explicit connection between a magnetically induced ring current and electron delocalization.[37]

A number of questions now emerge when considering BN/CC COT isosteres in their T_1 states. If there is a variation in their Baird-aromaticity with regard to the aromaticity aspect considered, can this variation be rationalized? Are there structural factors that contribute to strong Baird-aromaticity in T_1 and others that contribute to the opposite? Besides **COT** and two $B_4N_4H_8$ isomers (Group 1, Figure 2), all possible isomers of BNC_6H_8, with eight-membered rings with tricoordinate B, N and C atoms (Group 2), were investigated. We also examined a selection of $B_2N_2C_4H_8$ isomers by which the importance of various structural features can be tested (Group 3), and one $B_3N_3C_2H_8$ isomer which corresponds to **B_4N_4COT-A** except for one CC segment (Group 4). Through systematic study, we can conclude that the magnetic aspect of Baird-aromaticity in these molecules seldom agrees with the other aspects of Baird-aromaticity, resembling what has earlier been observed for the Hückel-aromaticity in the S_0 states of $(N_6H_6)^{2+}$ and $C_2N_4H_6$.[36]

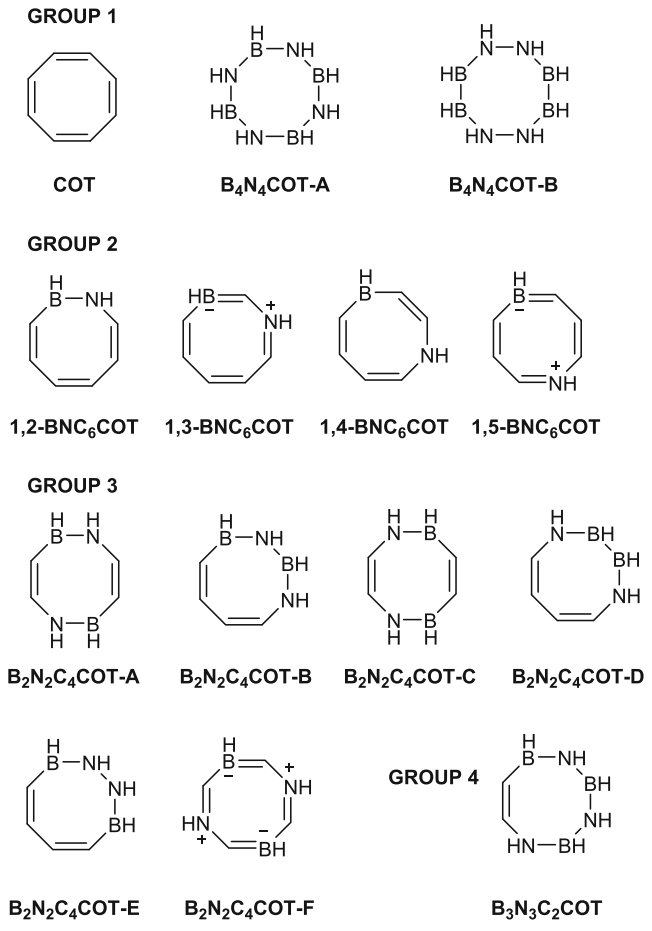

FIGURE 2 Structural formulas of the compounds investigated herein.

2 | COMPUTATIONAL METHODS

Geometry optimizations were carried out with the Gaussian 16[38] program package using different DFT functionals[39–45] and the 6-311G(d,p) valence triple-zeta basis set of Pople and co-workers.[46] Restricted and unrestricted Kohn-Sham DFT were used for, respectively, the closed-shell singlet ground state and the lowest ππ* triplet state. All wave functions were found to be stable, and the character of the stationary points as minima or saddle-points was checked through frequency calculations. The T_1 state geometries were optimized using either UBLYP, UB3LYP, UCAM-B3LYP, UOLYP and UωB97X-D, and the performances of these functionals were evaluated based on single-point UCCSD(T)/cc-pVTZ energies calculated at the optimized UDFT geometries.

The aromaticity analysis was based on computations at the UB3LYP/6-311G(d,p) level and applied a variety of indices and approaches: the electron density of delocalized bond (EDDB) function,[47,48] nucleus independent chemical shifts (NICS),[49,50] anisotropy of induced current density (ACID),[51] multicenter electron sharing indices (MCI),[52,53] the aromatic fluctuation index (FLU),[54] geometry-based harmonic oscillator model of aromaticity (HOMA)[55] and the isomerization stabilization energy (ISE) approach.[31,56] For HOMA the recently developed parameters for BN bonds ($\alpha = 72.03$ and $R_{opt} = 1.402$ Å)[55] have been used. A further detailed analysis of the magnetically induced current densities was carried out using the CTOCD-DZ (continuous transformation of the origin of current density method –diamagnetic zero) method.[57–60] The external magnetic field was applied perpendicularly to the molecular plane. The current density maps were plotted 1 bohr above the ring plane by setting clockwise/counterclockwise circulations to represent diatropic/paratropic current densities. The bond current strengths were obtained by numerical integration of the current densities passing through a rectangle bisecting the bond center. The integration rectangle starts from the ring center and extends 5 bohr from the bond center outside the molecular ring. This rectangle spreads 5 bohr above and 5 bohr below the ring plane. Ring current strengths (J, in nA T^{-1}) were calculated as the average of all bonds in the given ring.

3 | RESULTS AND DISCUSSION

The overarching aim of our study is to explore the T_1 state Baird-aromaticity of various BN/CC isosteres of COT using different types of indices and to determine the cause of the differences observed. We split the analysis into three sections; (*i*) a first comparison between **COT** and the two $B_4N_4H_8$ isomers in their T_1 states, followed by (*ii*) an analysis of the Baird-aromatic character of the T_1 states of azaboraCOTs with partial CC-to-BN exchange, and finally, (*iii*) a detailed exploration of the magnetically induced current densities of S_0 state borazine and selected T_1 state azaboraCOTs in order to identify causes for the difference in the aromaticity assessments from magnetic vs. electronic and energetic indices. The results discussed come from calculations with the UB3LYP functional as this DFT functional provided the best geometries when benchmarked with single-point UCCSD(T)/cc-pVTZ energies calculated at optimized UDFT T_1 state geometries (see the Supporting Information, p. 3). All azaboraCOTs investigated, except one, are planar in their T_1 states. The exception is **$^3B_3N_3C_2$COT** which adopts two different puckered conformers in T_1. For the other azaboraCOTs, geometry optimizations always lead to fully planar conformers, i.e., only higher-energy conformers with puckered eight-membered rings were found on the T_1 potential energy surfaces (PESs). Yet, azaboraCOTs with *E*,*Z*,*Z*,*Z* configurations have puckered minima in their S_0 states, but interestingly, in T_1 they either rearrange to the planar all-*Z* isomers or remain puckered and of higher energy (see Supporting Information, p. 6).

^{3}COT* versus *two $^3B_4N_4$COT isomers: In the S_0 state, **B_4N_4COT-A** exists in only one conformer, a planar D_{4h} symmetric structure with B-N bonds of 1.430 Å, in contrast to the highly puckered structure of two borazocines earlier determined crystallographically, which have *t*Bu substituents at the N and either isothiocyanate or methyl substituents at the B atoms[33,61] (see Supporting Information, p. 8). Isomer **B_4N_4COT-B** in S_0 exists in two conformers, both of which puckered; one C_2 symmetric of low energy and a second with no symmetry and a relative energy of 31 kcal/mol (Table S4). In T_1, on the other hand, both isomers adopt a planar and highly symmetric structure (Figure 3A), similar to **^{3}COT**, yet **$^3B_4N_4$COT-B** is 128.7 kcal/mol higher in energy than **$^3B_4N_4$COT-A**. Although the repulsion between electron pairs on adjacent N atoms and between holes on adjacent B atoms in

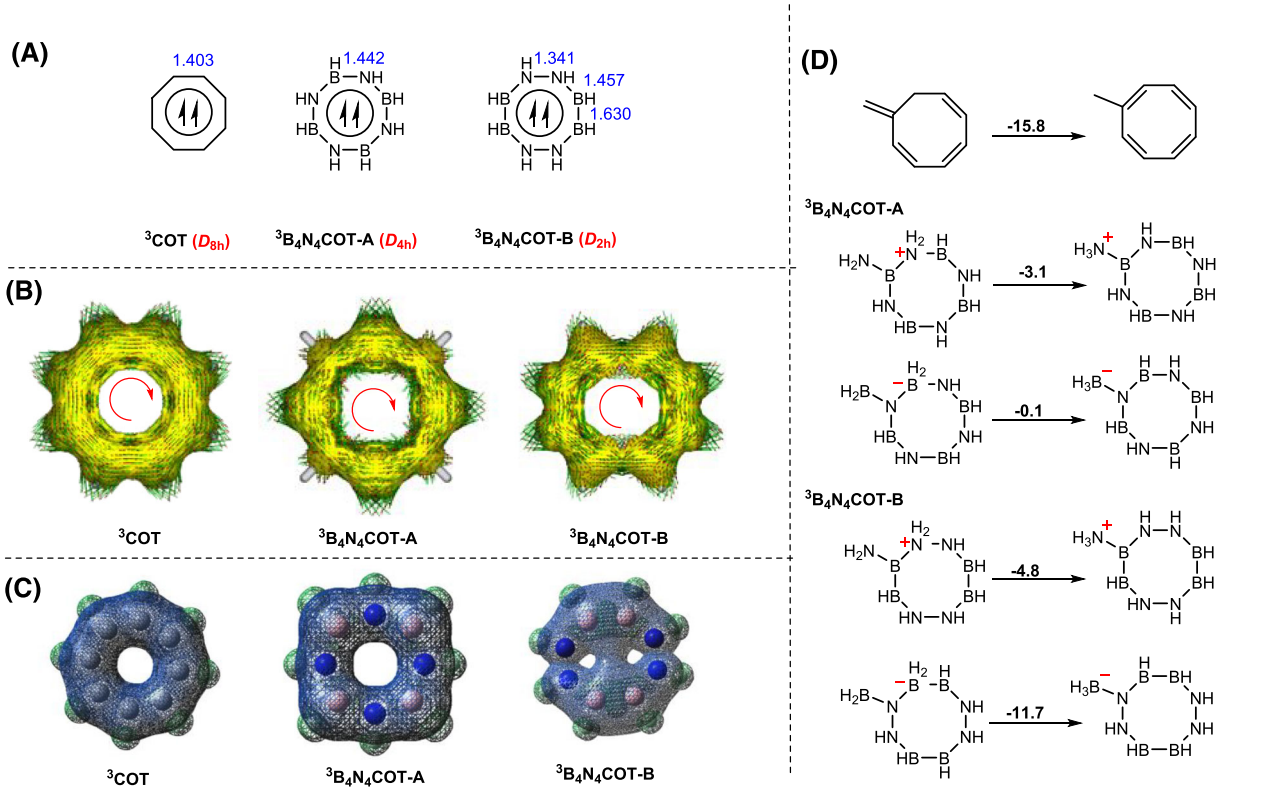

FIGURE 3 (A) Structural formula, optimized bond length (blue color) in Å and symmetry (in brackets) of **^{3}COT**, **$^3B_4N_4$COT-A** and **$^3B_4N_4$COT-B**. (B) ACID plots for the eight-membered ring compounds in their T_1 states at UB3LYP/6-311G(d,p) level (full ACID plots are available in the Supporting Information, Figures S8–S21). (C) Plots of the spin densities (isovalues at 0.0004 e/Å^3). (D) ISE values (kcal/mol) for methyl substituted **^{3}COT** and of H_3N^+ and H_3B^- substituted **$^3B_4N_4$COT-A** and **$^3B_4N_4$COT-B.**

$^3B_4N_4$COT-B may strengthen the dative B=N π-bond character, it will not increase the Baird-aromaticity as there can be no N=N and B=B double bonds as required for the second Kekulé-type resonance structure. Another notable feature is the much higher triplet energies ($E(T_1)$) of **B_4N_4COT-A** and **B_4N_4COT-B** than of **COT** (Table 1), a feature that indicates less aromatic stabilization in the T_1 states of the two $B_4N_4H_8$ isomers than that of **^{3}COT** (in S_0, the three molecules are either nonaromatic or weakly antiaromatic, see Table S5).

Normal B-N single and double bond lengths are, respectively, 1.564 and 1.363 Å,[7] which means that the B-N bonds of **$^3B_4N_4$COT-A** (all 1.442 Å, Figure 3A) are intermediate between single and double bonds. In **$^3B_4N_4$COT-B** the B-N bonds are just slightly longer than in the more stable isomer. The geometry-based HOMA values of **^{3}COT**, **$^3B_4N_4$COT-A** and **$^3B_4N_4$COT-B** are 0.944, 0.884 and 0.608, respectively, indicating a similar geometric aromaticity of **$^3B_4N_4$COT-A** as of borazine in S_0, but a more modest aromaticity of **$^3B_4N_4$COT-B**. However, a caveat with the usage of HOMA for Baird-aromaticity assessments is the lack of reference bond lengths and parameters for species in electronically excited states as it was developed for the S_0 state. Therefore, as an additional geometric-energetic aromaticity indicator, we considered the lowest vibrational modes, which for each of the three molecules is an out-of-plane vibration. The energy penalty for distorting a strongly aromatic compound out of planarity is normally significant. Indeed, **^{3}COT** has an out-of-plane vibration at 146 cm^{-1} while the corresponding vibrations for **$^3B_4N_4$COT-A** and **$^3B_4N_4$COT-B** are, respectively, 60 and 68 cm^{-1}. Yet, for benzene and borazine in S_0 the out-of-plane vibrations occur at much higher values of 412 and 291 cm^{-1} (they are also the lowest vibrations for these molecules), but when going to larger cycles there is a gradual increase in angle strain which renders the PESs for puckering (and aromaticity loss) more shallow. This becomes clear from the tropylium cation (**Trp$^+$**) and **COT** dication (**COT^{2+}**) in their Hückel-aromatic S_0 states, as these species have (much) smaller out-of-plane vibrational frequencies (222 and 35 cm^{-1}, respectively) than benzene. Indeed, it is interesting that **^{3}COT** has a higher out-of-plane vibrational frequency than **COT^{2+}**, indicating a larger energy penalty for out-of-plane deformations in the former (and a higher degree of aromaticity). Thus, it becomes apparent that **$^3B_4N_4$COT-A** and **$^3B_4N_4$COT-B** have slightly stronger preferences for planarity than **COT^{2+}** which is generally considered as Hückel-aromatic.

Next, we analyzed the magnetic aromaticity aspect. The $NICS(1)_{zz}$ values of **^{3}COT**, **$^3B_4N_4$COT-A** and **$^3B_4N_4$COT-B** are, respectively, -32.4, -19.3 and -16.3, suggesting that **^{3}COT** is the most Baird-aromatic but that both **B_4N_4COT** isomers in their T_1 states are significantly aromatic. One may argue that the negative NICS value of **B_4N_4COT-A** stems from local circulations at the N atoms, resembling what has been observed for the cyclic $(HF)_3$ complex where local circulations at the three HF molecules lead to a negative NICS in the ring center (-2.94)[62] and a false "aromaticity."[63] However, the ACID plots of **^{3}COT**, **$^3B_4N_4$COT-A** and **$^3B_4N_4$COT-B** reveal that all three compounds have true diatropic ring currents (Figure 3B), motivating the classification of the two $B_4N_4H_8$ isomers as Baird-aromatic based on the magnetic aspect. In contrast, borazine in S_0 has a $NICS(1)_{zz}$ value of merely -5.9 (Table 2), and the current density plot reveals a significantly weakened ring current and localized circulations at the three N atoms.[10] Here it should be noted that the borazocine dianion in S_0 earlier was observed to exhibit a strong diatropic ring current,[34] and with two electrons in both the HOMO and LUMO of the neutral borazocine, the Hückel aromaticity of the dianion can be related to the Baird-aromaticity of **$^3B_4N_4$COT-A** having one electron in each of these two orbitals.

The isomerization stabilization energies (ISEs) of **^{3}COT**, **$^3B_4N_4$COT-A** and **$^3B_4N_4$COT-B** were also calculated (Figure 3D). Whereas **^{3}COT** is clearly Baird-aromatic with a negative ISE similar to the value earlier reported by Zhu, An and Schleyer (-15.6 kcal/mol),[31] **$^3B_4N_4$COT-A** behaves as a non-aromatic species since its two ISE values are close to zero. Interestingly, the ISE values of the latter are even smaller than those of borazine in S_0 (Tables 1 and 2). The ISE values of **$^3B_4N_4$COT-B** (-11.7 and -4.8 kcal/mol), on the other hand, reveal a

TABLE 1 Triplet energies ($E(T_1)$), and T_1 state HOMA, ν_{oop}, $NICS(1)_{zz}$, ΔISE, $EDDB_H(\pi)$, FLU and MCI values of **^{3}COT**, **$^3B_4N_4$COT-A** and **$^3B_4N_4$COT-B**[a]

Compound	$E(T_1)$	HOMA	ν_{oop}	$NICS(1)_{zz}$	ISE	$EDDB_H(\pi)$	FLU	MCI
^{3}COT	15.5	0.944	146	−32.4	−15.8	7.45 (93%)	0.001	0.0275
$^3B_4N_4$COT-A	102.2	0.884	60	−19.3	−3.1, −0.1	5.95 (74%)	0.237	0.0016
$^3B_4N_4$COT-B	76.3	0.608	68	−16.3	−11.7, −4.8	4.15 (52%)	0.053	0.0013

[a]$E(T_1)$ and ΔISE in kcal/mol.

TABLE 2 Triplet energies ($E(T_1)$), and S_0 state HOMA, ν_{oop}, NICS(1)$_{zz}$, ΔISE, EDDB$_H(\pi)$, FLU and MCI values of benzene, borazine, the tropylium cation (**Trp**$^+$) and COT dication[a]

Compound	$E(T_1)$	HOMA	ν_{oop}	NICS(1)$_{zz}$	ISE	EDDB$_H(\pi)$	FLU	MCI
Benzene (S_0)	111.4	0.992	412	−29.3	−34.2	5.33 (89%)	0.0000	0.0726
Borazine (S_0)	122.0	0.946	291	−5.9	−12.6, −6.7	3.44 (57%)	0.3105	0.0026
Trp$^+$ (S_0)	77.0	0.985	222	−26.5	−30.5	5.62 (94%)	0.0005	0.0575
COT^{2+} (S_0)	41.0	0.897	35	−25.4	−5.9	5.86 (98%)	0.0023	0.0412

[a]$E(T_1)$ and ΔISE in kcal/mol.

more complex situation as one of the values approaches that of **^{3}COT** (-15.8 kcal/mol). This may suggest some T_1 state Baird-aromaticity, but the very high relative energy of **^{3}B$_4$N$_4$COT-B** (128 kcal/mol) speaks against such an interpretation. For comparison, the aromatic archetype benzene has been found to be the lowest in energy among 198 C_6H_6 isomers, 35 kcal/mol lower in energy than the second most stable isomer, fulvene.[64] Here, it is notable that the second ISE value of **^{3}B$_4$N$_4$COT-B** is low and representative of nonaromaticity.

The fourth aromaticity aspect, the electronic aspect, reinforces the interpretation of the ISE values. The FLU values of all molecules are non-zero but it is more than 200 times larger for **^{3}B$_4$N$_4$COT-A** than for **^{3}COT**, while in case of **^{3}B$_4$N$_4$COT-B** it is 50 times larger than that of **^{3}COT**. Thus, FLU indicates that the two isomers of **^{3}B$_4$N$_4$COT,** when compared to **^{3}COT**, are non-aromatic. Additionally, the MCI values of both **^{3}B$_4$N$_4$COT-A** and **^{3}B$_4$N$_4$COT-B** are only a tenth of the value of **^{3}COT**, underlining the conclusion based on FLU of weak or no aromaticity. To further explore the delocalization, we calculated EDDB$_H(\pi)$ values of **^{3}COT**, **^{3}B$_4$N$_4$COT-A** and **^{3}B$_4$N$_4$COT-B.** It is clear that the π-electrons of **^{3}COT** are nearly completely delocalized with an EDDB$_H(\pi)$ value 7.45 (93% of eight π-electrons). For **^{3}B$_4$N$_4$COT-A** and **^{3}B$_4$N$_4$COT-B**, EDDB$_H(\pi)$ indicates that the electrons are less delocalized as 5.95 (74%) and 4.15 (52%) of the π-electrons are delocalized over the octagon. On the other hand, **^{3}B$_4$N$_4$COT-A** exhibits more extensive delocalization than borazine in S_0 where 3.44 π-electrons (57%) are delocalized over the hexagon, which gives support to the qualitative hypothesis put forth above that borazocine can be more Baird-aromatic in T_1 than borazine is Hückel-aromatic in S_0. Still, the extent of π-electron delocalization is lower than that of **^{3}COT**. Finally, one can also observe visually that the spin density is extensively delocalized in **^{3}B$_4$N$_4$COT-A** (Figure 3C), yet slightly less so than in **^{3}COT** if one considers plots with gradually larger spin density isovalues (Table S6).

In summary, while **^{3}COT** indisputably Baird-aromatic according to each of the four aromaticity aspects (magnetic, geometric, energetic and electronic) this is not the case for the two **^{3}B$_4$N$_4$COT** species because they are only unquestionably Baird-aromatic according to the magnetic aspect. A question is at which azaboraCOTs the split between the various aspects of T_1 state Baird-aromaticity emerge as one goes from **^{3}COT** to **^{3}B$_4$N$_4$COT**?

Intermediate azabora COTs in their T_1 states: We now successively replace two C atoms of COT with one B and one N atom (Groups 2 – 4, Figure 2). All possible BNC_6H_8 isomers with eight-membered rings (**^{3}1,2-BNC$_6$COT**, **^{3}1,3-BNC$_6$COT**, **^{3}1,4-BNC$_6$COT** and **^{3}1,5-BNC$_6$COT**), six different $B_2N_2C_4H_8$ isomers (**^{3}B$_2$N$_2$C$_4$COT-A** to **^{3}B$_2$N$_2$C$_4$COT-F**), and finally one $^3B_3N_3C_2H_8$ isomer, were examined. While there can be dative bonding in the S_0 states of **1,2-** and **1,4-BNC$_6$COT** leading to zwitterionic resonance structures, such structures are the only closed-shell structures that can be formulated for **1,3-** and **1,5-BNC$_6$COT** as they are mesoionic,[65–67] i.e., negative and positive charges must either be placed on the B and N atoms or at adjacent C atoms (Figure S2). Also, **B$_2$N$_2$C$_4$COT-F** is a mesoionic compound.

Of the four **BNC$_6$COT** isomers, **1,2-BNC$_6$COT** is the thermodynamically most stable in both S_0 and T_1. The second most stable in S_0 is **1,4-BNC$_6$COT** at a relative energy of 29.4 kcal/mol, while this isomer is the least stable in the T_1 state 30.6 kcal/mol above **^{3}1,2-BNC$_6$COT** (Table S8). Clearly, the possibility for a direct BN π-dative bond in **1,2-BNC$_6$COT** is strongly stabilizing in S_0 (Figure S2), similar to the situation for the three azaborines (BNC_4H_6) in S_0 where the 1,2-azaborine is the most stable isomer.[68] In contrast, the **1,3-** and **1,5-BNC$_6$COT** isomers, being mesoionic, are markedly destabilized in this state. In T_1, on the other hand, they are of lower relative energy than **1,4-BNC$_6$COT** since they can be described as composed of two polyenyl radical segments and neutral B and N atoms (Figure S2). Consequently, the $E(T_1)$ of **1,3-** and **1,5-BNC$_6$COT** are very low due to their extensive destabilization in S_0 (Tables 3 and S8). The $E(T_1)$ of **1,2-** and **1,4-BNC$_6$COT** are higher yet still much more similar to that of **COT** than to that of

TABLE 3 Triplet energies $E(T_1)$, and the T_1 state ν_{oop}, ΔISE, $NICS(1)_{zz}$, $EDDB_H(\pi)$, FLU and MCI values of **1,2-BNC$_6$COT**, **1,3-BNC$_6$COT**, **1,4-BNC$_6$COT**, **1,5-BNC$_6$COT**, **B$_2$N$_2$C$_4$COT-A**, **B$_2$N$_2$C$_4$COT-B**, **B$_2$N$_2$C$_4$COT-C**, **B$_2$N$_2$C$_4$COT-D**, **B$_2$N$_2$C$_4$COT-E**, **B$_2$N$_2$C$_4$COT-F** and **B$_3$N$_3$C$_2$COT** at UB3LYP/6-311G(d,p) level

Compound	$E(T_1)$[a]	ν_{oop}[b]	HOMA	ISE[c]	$NICS(1)_{zz}$	$EDDB_H(\pi)$	FLU	MCI
^{3}1,2-BNC$_6$COT	26.7	120	0.802	−7.7[d]	−20.6	4.85 (61%)	0.054	0.0057
^{3}1,3-BNC$_6$COT	3.7	111	0.706	−7.8[d]	−20.2	4.59 (57%)	0.029	0.0026
^{3}1,4-BNC$_6$COT	27.9	97	0.703	−10.5[d]	−23.9	5.03 (63%)	0.031	0.0029
^{3}1,5-BNC$_6$COT	1.4	94	0.698	−7.7[d]	−18.1	5.06 (63%)	0.035	0.0029
^{3}B$_2$N$_2$C$_4$COT-A	48.2	115	0.932	−11.2[d]	−24.0	5.47 (68%)	0.087	0.0031
^{3}B$_2$N$_2$C$_4$COT-B	38.7	86	0.832	−4.4[d]	−12.3	3.69 (46%)	0.131	0.0015
^{3}B$_2$N$_2$C$_4$COT-C	43.1	91	0.842	−12.8[d]	−16.6	3.26 (41%)	0.119	0.0027
^{3}B$_2$N$_2$C$_4$COT-D	26.4	112	0.862	−6.9[d]	−16.5	4.32 (54%)	0.027	0.0012
^{3}B$_2$N$_2$C$_4$COT-E	46.1	86	0.714	−2.6[d]	−15.4	3.57 (45%)	0.098	-0.0006
^{3}B$_2$N$_2$C$_4$COT-F	2.1	126	0.664	−19.2, −16.0[e]	−24.3	5.56 (69%)	0.036	0.0023
^{3}B$_3$N$_3$C$_2$COT	56.5	-[f]	0.846	-[g]	0.9	2.62 (33%)	0.215	0.0001

[a] $E(T_1)$ in kcal/mol.
[b] Frequency for the out-of-plane vibrational mode in cm^{-1}.
[c] ISE values in kcal/mol.
[d] Calculated as T_1 energy differences between the most stable isomer of the nonaromatic isomers and the most stable isomer among the aromatic ones. Details on the ISE equations are given in the Supporting Information, p. 15-29.
[e] Calculated based on single ISE reactions, one with methylene/methyl substitution at N and one at B.
[f] **^{3}B$_3$N$_3$C$_2$COT** is markedly puckered and has no out-of-plane vibrational mode.
[g] The formally aromatic isomer of this compound adopts a strongly puckered conformation in T_1 and an ISE value is therefore not meaningful.

B$_4$N$_4$COT-A (Table 1). Indeed, the rather low $E(T_1)$ of **1,2-** and **1,4-BNC$_6$COT** can indicate some aromatic stabilization in T_1.

The effect of replacing two C atoms with one B and one N atom on the geometric aspect of Baird-aromaticity is interesting. Compared to both **^{3}COT** and **^{3}B$_4$N$_4$COT**, the HOMA values of the four **^{3}BNC$_6$COT** isomers are slightly lower (0.70–0.80, Table 3), yet still indicative of clear aromatic character. The CC bond lengths and the modest BLA in the hexatriene carbon segment (1.386–1.433 Å, Figure S2) of **^{3}1,2-BNC$_6$COT** and in the butadiene segment of **^{3}1,4-BNC$_6$COT** (1.386 – 1.419 Å) also suggest π-electron delocalization indicative of aromatic character, and so do the out-of-plane vibrational frequencies ν_{oop} which are intermediate between those of **^{3}COT** and **^{3}B$_4$N$_4$COT-A** (Table 3).

Interestingly, the $NICS(1)_{zz}$ values for three of the four **^{3}BNC$_6$COT** isomers resemble the values for **^{3}B$_4$N$_4$COT-A** and **^{3}B$_4$N$_4$COT-B** despite that they have six C atoms and may be expected to mainly resemble **^{3}COT**. Only one isomer, **^{3}1,4-BNC$_6$COT**, has a NICS value that tends towards that of **^{3}COT**. Unsurprisingly, the ACID plots reveal diatropic ring currents in all four isomers in their T_1 states (Figure 4), similar as for **^{3}B$_4$N$_4$COT-A** and **^{3}B$_4$N$_4$COT-B**.

However, opposite to the magnetic and geometric aromaticity indicators, the electronic indices FLU, MCI and $EDDB_H(\pi)$ tell that the four $^3BNC_6H_8$ isomers are at most weakly aromatic when compared to **^{3}COT**. The three electronic indices vary as to which isomer exhibits a weak aromatic character and which ones are nonaromatic. MCI indicates that **1,2-BNC$_6$COT** may have a weak aromatic character with an MCI value of 20% of that of **^{3}COT**, while FLU indicates that **^{3}1,3-BNC$_6$COT** may have a modest aromatic character, although the FLU value is significantly higher than that of **^{3}COT** (0.029 vs. 0.001). With regard to the $EDDB_H(\pi)$ values they are distinctly lower than that of **^{3}B$_4$N$_4$COT-A**, and the percentage of delocalized π-electrons in the four **^{3}BNC$_6$COT** isomers (57 – 63%) is the same or just slightly higher than that of borazine in S_0 (57%) and considerably lower than that of the Baird-aromatic **^{3}COT** (93%).

For the ISE values, it should be stressed that we selected only ISE reactions in which the same number of bond types exist on the reactant (nonaromatic) and product (aromatic) side, as the ISE values otherwise incorporate both aromatic stabilization energies and differences in bond strengths. Thus, an H atom that migrates by a 1,3-shift must transfer between either two C atoms, two B atoms, or two N atoms. A further caveat with the ISE values is the fact that the relative energies vary significantly among the non-aromatic isomers, as these are differently able to host a triplet diradical (some nonaromatic isomers can form resonance stabilized

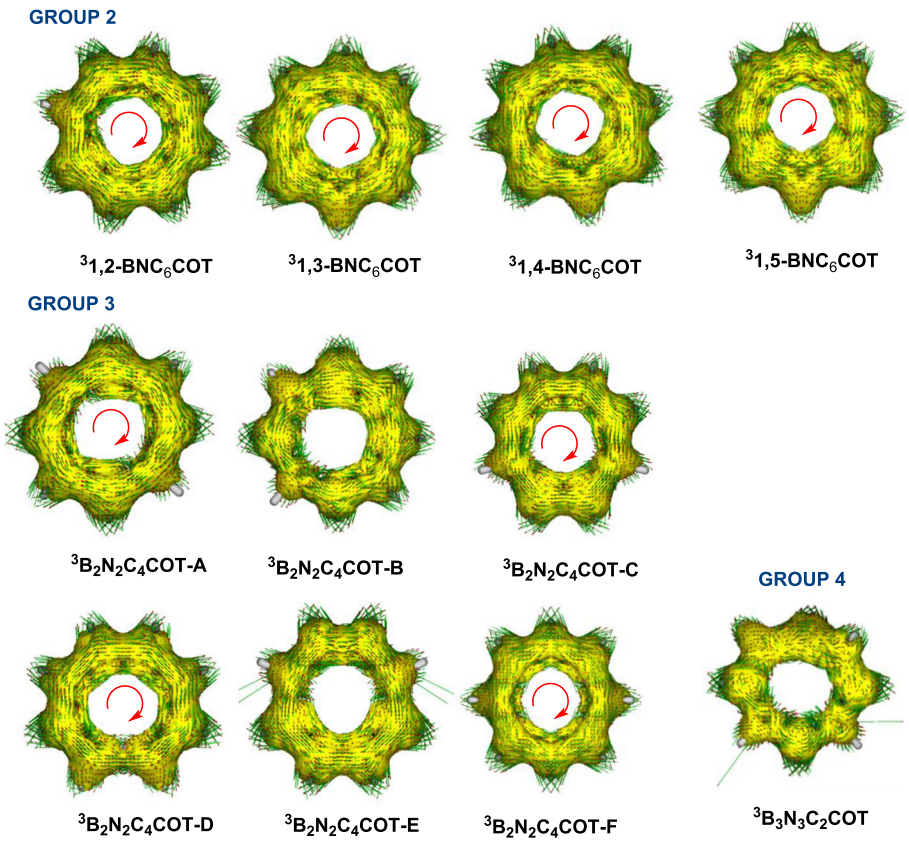

FIGURE 4 ACID plots of ^{3}**1,2-BNC$_6$COT**, ^{3}**1,3-BNC$_6$COT**, ^{3}**1,4-BNC$_6$COT**, ^{3}**1,5-BNC$_6$COT**, ^{3}**B$_2$N$_2$C$_4$COT-A**, ^{3}**B$_2$N$_2$C$_4$COT-B**, ^{3}**B$_2$N$_2$C$_4$COT-C**, ^{3}**B$_2$N$_2$C$_4$COT-D**, ^{3}**B$_2$N$_2$C$_4$COT-E**, ^{3}**B$_2$N$_2$C$_4$COT-F** and ^{3}**B$_3$N$_3$C$_2$COT** at UB3LYP/6-311G(d,p) level. The isodensity value is 0.03 e/Å^3 and the red arrow indicates the continuous circulation of small arrows throughout the plane of the ring. Full-scale ACID plots are given in Figures S8–S21.

polyenyl radical segments). Hence, the ISE values do not only describe the aromatic stabilization but also the extent of resonance stabilization in the non-aromatic isomers on the reactant side. Yet, if one considers the energy difference between the most stable non-aromatic and the most stable aromatic isomer among the **1,2-BNC$_6$COT** species in T_1 one gets an ISE value of -7.7 kcal/mol (Table 3), and for the **1,3-BNC$_6$COT** species we similarly calculate an ISE value of -7.8 kcal/mol. Since these ISE values are based on the most stable nonaromatic isomer they do not incorporate any internal destabilization within the nonaromatic isomer, and accordingly, should predominantly correspond to the lowering in energy due to aromatic stabilization when going from the nonaromatic to the aromatic isomer (for the complete list of ISE equations and relative energies see the ESI). From the ISE values calculated in this way it becomes clear that approximately half of the Baird-aromaticity has been lost when going from ^{3}**COT** to three of the ^{3}**BNC$_6$COT** while ^{3}**1,4-BNC$_6$COT** exhibits a smaller loss.

Now, returning to the question posed in the Introduction as to when (at which T_1 state azaboraCOT) the split between the magnetic versus electronic and energetic aromaticity aspects sets in, the split exists for the ^{3}**BNC$_6$COT** isomers. They exhibit significantly negative NICS values and diatropic ring currents (although not as strong as for ^{3}**COT**), but the values of the electronic indices differ markedly from those of ^{3}**COT**. Among the geometric and energetic indices, HOMA and ν_{oop} reveal values that are somewhat lower than those of ^{3}**COT**, yet still indicative of aromaticity. The ISE values, in contrast, tend towards non-aromaticity. Clearly, incorporation of just one pair of B and N atoms into the COT scaffold weakens Baird-aromaticity, which is most apparent via the electronic and energetic aromaticity aspects.

Going to the six ^{3}**B$_2$N$_2$C$_4$COT** isomers, isomers **A** and **F** exhibit stronger magnetic aromaticity than ^{3}**B$_4$N$_4$COT-A** according to NICS while the opposite is the case for the other isomers. The ν_{oop} of ^{3}**B$_2$N$_2$C$_4$COT-A** and **-F** are also similar to that of ^{3}**1,2-BNC$_6$COT**, and their percentage π-electron delocalization according to $EDDB_H(\pi)$ is high (68-69%) when compared to borazine in S_0, and approaching that of ^{3}**B$_4$N$_4$COT-A**. The four other ^{3}**B$_2$N$_2$C$_4$COT** isomers have $EDDB_H(\pi)$ values which are substantially lower than that of borazine in S_0. The FLU and MCI values also indicate that all investigated ^{3}**B$_2$N$_2$C$_4$COT** isomers lack aromatic character. Their ISE values of the first five ^{3}**B$_2$N$_2$C$_4$COT** isomers vary in the range -12.8 to -2.6 kcal/mol with **B$_2$N$_2$C$_4$COT-C** and **B$_2$N$_2$C$_4$COT-A** having some aromatic character. Unexpectedly, ^{3}**B$_2$N$_2$C$_4$COT-F** has more negative ISE values than ^{3}**COT**, yet, when evaluating the energetic impact of aromaticity one should also consider relative energies. The thermodynamically most stable **B$_2$N$_2$C$_4$COT** isomer

in both S_0 and T_1 is **$B_2N_2C_4$COT-B** (Table S9), whereas **$B_2N_2C_4$COT-F** is the absolutely least stable in both states (in the T_1 state it is 64 kcal/mol above **$^3B_2N_2C_4$COT-B**). I.e., despite significant Baird-aromatic character according to magnetic and geometric indices, it is of very high energy. The $E(T_1)$ of isomer **A** is high and intermediate between those of **COT** and **B_4N_4COT-A** while the $E(T_1)$ of the mesoionic **$B_2N_2C_4$COT-F** is minute. The other four $B_2N_2C_4H_8$ isomers considered have higher $E(T_1)$ energies, but at most slightly less than half that of **B_4N_4COT-A**.

Finally, among $B_3N_3C_2H_8$ species, we explore only the **$^3B_3N_3C_2$COT** isomer, which has a consecutive $(BN)_3$ segment. This molecule can be viewed as **B_4N_4COT-A** with one BN unit exchanged to a CC unit, and as noted, we could only locate puckered conformers (a planar C_s symmetric structure is a transition state for inversion between two equivalent puckered conformers and 2.2 kcal/mol higher in energy). Due to the puckered ring, the spin density is separated into two segments corresponding to separate radicals (Figure S6). Thus, **$^3B_3N_3C_2$COT** cannot be Baird-aromatic as supported by a very low electron delocalization throughout the ring, no ring current and a NICS value that suggests a lack of aromaticity (Table 3). Despite this, the geometric HOMA index (0.846) corresponds to a significant aromaticity.

Analysis of magnetically induced current densities: In this section we further explore borazine in S_0 and a selection of the azaboraCOTs which in their T_1 states have strong Baird-aromatic character according to the magnetic criteria. The total and the π-electron current density maps of borazine in S_0 and **$^3B_4N_4$COT-A** are displayed in Figure 5A–D. In the case of borazine in S_0, there are local currents around the N atoms instead of a significant global circulation. In contrast, in **$^3B_4N_4$COT-A** there are significant diatropic π-electron ring currents which are uniformly distributed over the molecular ring, and the separated current densities of **$^3B_4N_4$COT-A** (Figure 5E,F) clarifies that the π_α-electron current density has a somewhat stronger contribution than the π_β-electrons. Quantitative descriptions of the current density distributions are obtained from the integrated bond current strengths (Table 4), and the total π-electron ring current strength of **$^3B_4N_4$COT-A** is three times larger than that of borazine in S_0 and ∼60% that of **^{3}COT**, in line with the NICS values given above.

Interestingly, the replacement of two C atoms of **^{3}COT** by one N and one B atom, leading to **^{3}1,2-BNC$_6$COT** and **^{3}1,3-BNC$_6$COT**, results in π-electron currents which are approximately two thirds that of **^{3}COT** (Table 4 and Figure 6), i.e., only slightly larger than that of **$^3B_4N_4$COT-A**. Thus, it is not the sheer number of B and N atoms that is decisive for the current densities but rather the connectivity between the B, C and N atoms, which is also apparent from the isomeric azaboraCOTs **$^3B_2N_2C_4$COT-A** and **$^3B_2N_2C_4$COT-F**. Despite two B and two N atoms, these two compounds exhibit

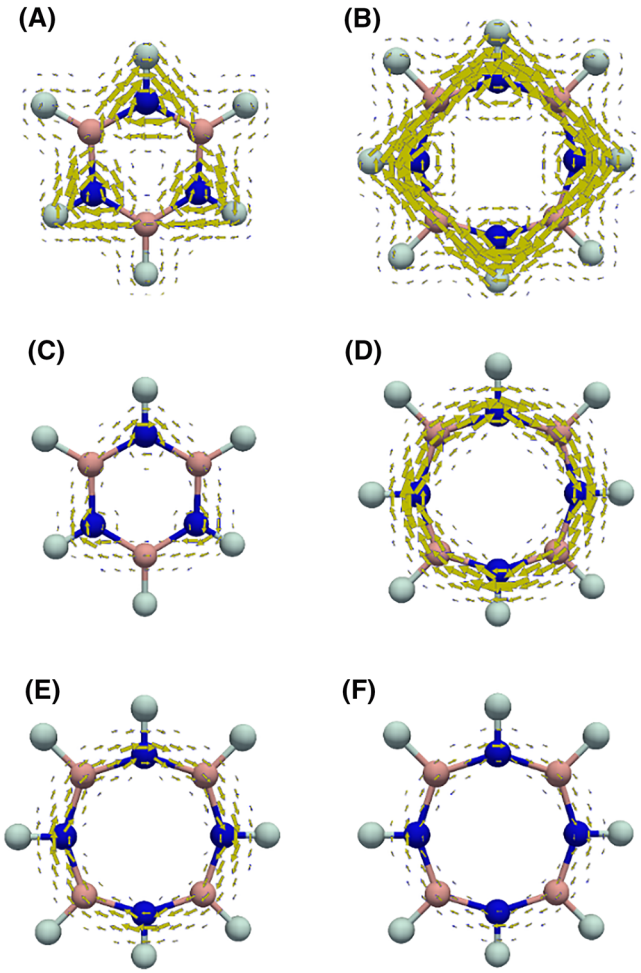

FIGURE 5 (A and B) Total (all electron) current density maps of, respectively, borazine in S_0 and **B_4N_4COT-A** in T_1. (C and D) π-electron current density maps of, respectively, borazine in S_0 and **B_4N_4COT-A** in T_1. (E and F) π-electron current density maps of **B_4N_4COT-A** dissected into, respectively, α- and β-electron contributions.

TABLE 4 Ring current strengths (J, in nA T^{-1}) calculated as the average of all bonds in the given ring

	All electrons	π-Total	π_α	π_β
Borazine (S_0)	3.6	3.2	1.6	1.6
^{3}COT	15.6	15.1	9.2	5.9
$^3B_4N_4$COT-A	9.7	9.2	5.4	3.7
$^3B_4N_4$COT-B	8.3	7.8	5.1	2.6
^{3}1,2-BNC$_6$COT	10.7	10.2	7.0	3.3
^{3}1,3-BNC$_6$COT	10.5	10.0	6.9	3.1
$^3B_2N_2C_4$COT-A	11.9	11.4	7.2	4.1
$^3B_2N_2C_4$COT-F	11.9	11.5	7.4	4.1

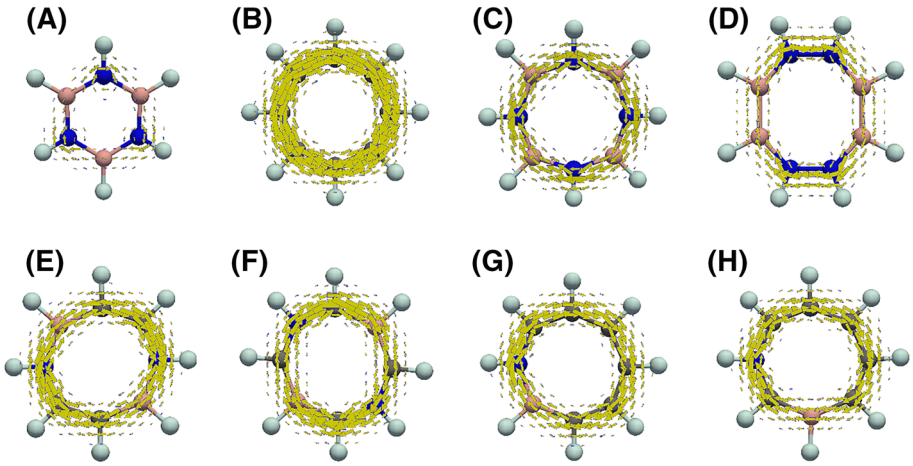

FIGURE 6 π-Electron current density maps of (A) borazine in S_0, (B) ^{3}**COT**, (C) ^{3}**B$_4$N$_4$COT-A**, (D) ^{3}**B$_4$N$_4$COT-B**, (E) ^{3}**1,2-BNC$_6$COT**, (F) ^{3}**1,3-BNC$_6$COT**, (G) ^{3}**B$_2$N$_2$C$_4$COT-A** and (H) ^{3}**B$_2$N$_2$C$_4$COT-F.**

stronger current densities than ^{3}**1,2-BNC$_6$COT** and ^{3}**1,3-BNC$_6$COT** (Table 4). Clearly, the azaboraCOT with the strongest π-electron current densities is not the one with the structurally closest resemblance to ^{3}**COT** but instead the ^{3}**B$_2$N$_2$C$_4$COT-F** with a high relative energy (64 kcal/mol) compared to the most stable isomer (^{3}**B$_2$N$_2$C$_4$COT-B**). A similar finding was made earlier for azaborines (BNC_4H_6) in their S_0 states where the least stable isomer (1,3-azaborine) displayed the highest aromatic character.[68]

To resolve the cause of the differences in current densities, we related these to virtual transitions from the occupied to unoccupied orbitals.[69] The orbital diatropic and paratropic contributions to the total current density come from, respectively, virtual translational and rotational orbital transitions. The weight of the given orbital transition becomes more pronounced as the energy gap between the given occupied-virtual orbital pair decreases. Hence, the magnetic aspect of aromaticity does not merely reflect the electron configuration(s) that correspond to the state under consideration (here, S_0 or T_1) as it also involves virtual transitions to unoccupied orbitals as a means for the molecule to respond to the applied magnetic field being an external perturbation.

Borazine in S_0 belongs to the D_{3h} point group (Figure 7). In this point group, the in-plane translations ($T_{x,y}$) have e' symmetry, whereas the in-plane rotation (R_z) has a'$_2$ symmetry. Our calculations showed that π-electron currents in borazine in S_0 are dominated by the contribution of the e" level. The HOMO-LUMO (e" to e") excitation is both rotationally and translationally allowed since the product e" × e" = a'$_1$ + a'$_2$ + e' contains the symmetries of both $T_{x,y}$ and R_z, and this explains why the π-electron currents in borazine in S_0 are very weak.

Now going to the T_1 state, the α- and β-electrons are considered separately within the unrestricted formalism.

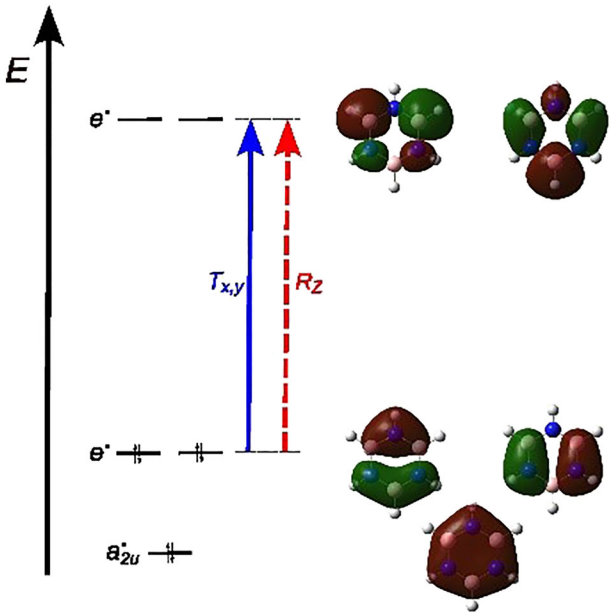

FIGURE 7 Frontier orbital energy levels of borazine in S_0. Blue arrows represent the main translational transitions and red dashed arrows represent the main rotational transitions.

^{3}**COT** has D_{8h} symmetry (Figure 8), whereby the in-plane translations ($T_{x,y}$) have e_{1u} symmetry and the in-plane rotation (R_z) has a_{2g} symmetry. For the π_α-electrons the main contribution to the induced currents comes from the excitation e_{2u} to e_{3g}, since the product $e_{2u} \times e_{3g} = e_{1u} + e_{3u}$ contains the symmetry of in-plane translations, which solely contributes to diatropic currents. Similarly, within π_β-electrons the main contribution comes from the e_{1g} to e_{2u} excitation ($e_{1g} \times e_{2u} = e_{1u} + e_{3u}$), also giving rise exclusively to diatropic currents. As a consequence, ^{3}**COT** displays a strong Baird-aromatic character.

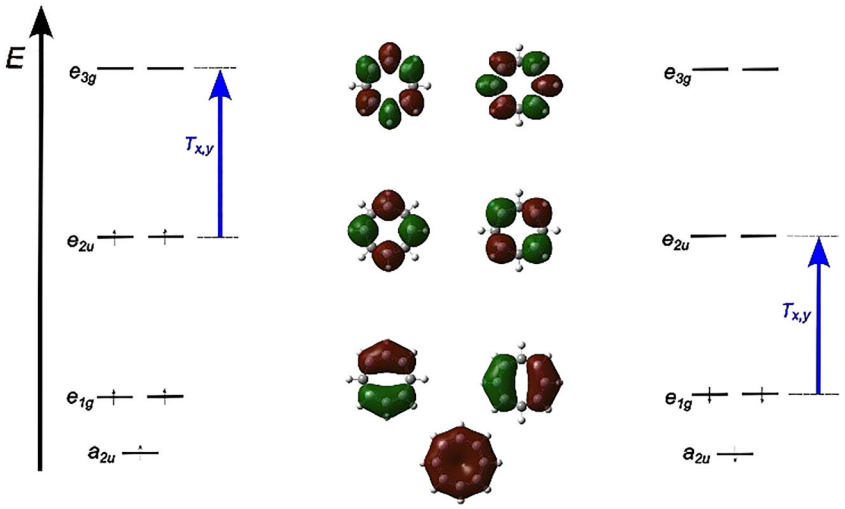

FIGURE 8 Frontier orbital energy levels of **^{3}COT**. Blue arrows represent the main translational transitions. As there are no rotational transitions, the diagram contains no red dashed arrows. The variation of energy between α and β levels is ignored.

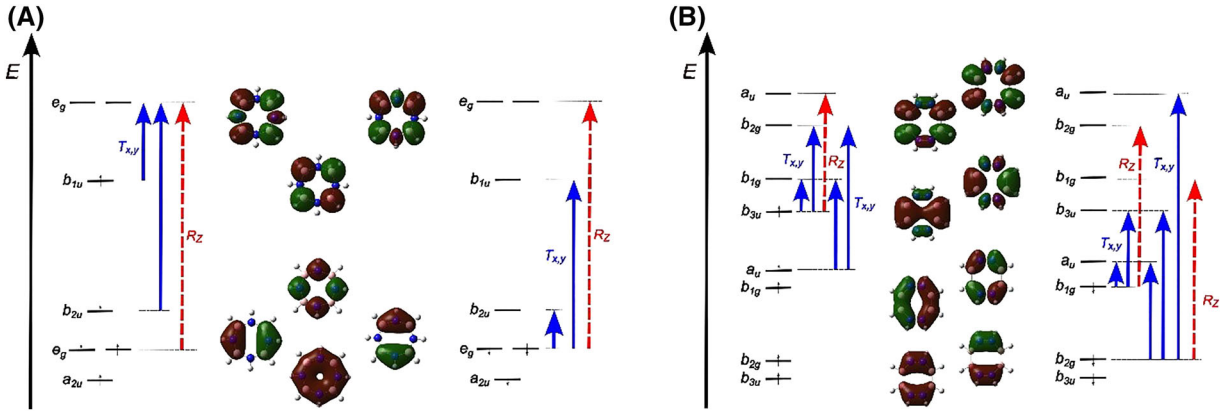

FIGURE 9 Frontier orbital energy levels of (A) **^{3}B$_4$N$_4$COT-A** and (B) **^{3}B$_4$N$_4$COT-B**. Blue arrows represent the main translational transitions and red dashed arrows represent the main rotational transitions. The variation of energy between α and β levels is ignored.

A further feature of the D_{8h} symmetry is the fact that all occupied π-orbitals except the lowest are doubly degenerate (Figure 8). Within each of those degenerate pairs, one can carry out unitary transformations, which for the nonbonding orbital pair (e_{2u}), filled only with π_α-electrons, implies that those MOs can be transformed between localized representations (shown in Figure 8) and delocalized representations (Figure S22). Thus, both the two π_α-electrons in the α-spin orbital manifold and the two holes in the β-spin orbital manifold are perfectly delocalized, providing for a high degree of Baird-aromaticity.

Going to the D_{4h} symmetric **^{3}B$_4$N$_4$COT-A** (Figure 3A), the in-plane translations ($T_{x,y}$) have e_u symmetry and the in-plane rotation (R_z) has a_{2g} symmetry (Figure 9). Our numerical results show that π_α-electron currents are dominated by b_{2u} and b_{1u} SOMOs, while the π_β-electron currents solely come from the degenerate e_g level. The π_α-electron currents arise from the excitations from b_{2u} and b_{1u} to e_g. These excitations contribute to diatropic currents since the products $b_{2u} \times e_g = b_{1u} \times e_g = e_u$ contain the symmetry of in-plane translations. It is further noteworthy that our calculations showed that the π_α-electron e_g level solely gives a paratropic current density contribution, which, however, is very weak. This paratropic contribution comes from the transition to the virtual e_g level, since the product $e_g \times e_g = a_{1g} + a_{2g} + b_{1g} + b_{2g}$ contains the symmetry of the in-plane rotation (a_{2g}). The π_β-electron currents arise from excitations from the degenerated e_g level to b_{2u} and b_{1u} which contribute to diatropic currents. On the other hand, there is a simultaneous excitation e_g to e_g which is rotationally allowed and reduces the overall diatropic contribution of the e_g level. This can explain why π_β-electron currents are weaker than that of π_α-electrons. Combined, in **^{3}B$_4$N$_4$COT-A** there are both translational (diatropic) and rotational (paratropic) transitions, yet the diatropic are significantly stronger and the situation

tends towards that of **^{3}COT** where there are only translational transitions. Here it is notable that strong diatropic ring currents were earlier observed for the borazocine dianion in S_0,[34,35] a species that resembles **^{3}B$_4$N$_4$COT-A** as the same virtual excitations are involved in the two species, however, with two electrons in the b_{2u} and b_{1u} orbitals of the first while one π_α electron in each of these orbitals of the latter.

At this point, it is relevant to ask, why is the π-electron delocalization of **^{3}B$_4$N$_4$COT-A**, at an orbital level, lower than that of **^{3}COT**? In contrast to **^{3}COT**, **^{3}B$_4$N$_4$COT-A** is D_{4h} symmetric, and thereby the former pair of degenerate nonbonding orbitals (e_{2u}) has turned into the nondegenerate b_{2u} and b_{1u}, which are localized on, respectively, the four N atoms and the four B atoms (Figure 9A). This orbital feature has direct consequences for the π-electron delocalization of **^{3}B$_4$N$_4$COT-A** (and its Baird-aromaticity) as it is no any longer possible to transform between localized and delocalized representations of the highest occupied π_α-orbitals. The azaboraCOT **^{3}B$_2$N$_2$C$_4$COT-F**, which is C_2 symmetric, also has no degenerate frontier orbitals, but for this molecule the nondegenerate a_u and b_{3u} orbitals are much closer in energy and resemble the degenerate e_{2u} orbital level in **^{3}COT** (Figure S23).

Finally, **^{3}B$_4$N$_4$COT-B** has D_{2h} symmetry (Figure 9), and in this point group the in-plane translations ($T_{x,y}$) have b_{2u} and b_{1u} symmetries, whereas the in-plane rotation (R_z) has b_{3g} symmetry. The induced π_α-electron currents are dominated by excitations from b_{3u} and a_u SOMOs, while π_β-electron currents mainly come from the b_{1g} and b_{2g} levels. The excitations from the b_{3u} SOMO to b_{1g} and b_{2g} are translationally allowed ($b_{3u} \times b_{1g} = b_{2u}$ and $b_{3u} \times b_{2g} = b_{1u}$), whereas the excitation to the a_u level is rotationally allowed ($b_{3u} \times a_u = b_{3g}$). The latter one diminishes the overall diatropic contribution of the b_{3u} SOMO level. The excitations from the π_α-electron a_u SOMO to b_{1g} and b_{2g} are translationally allowed and this orbital gives solely diatropic contribution. In the π_β-system there are excitations from the b_{1g} SOMO to a_u and b_{3u}, which are translationally allowed, while the excitation to b_{2g} level is rotationally allowed ($b_{1g} \times b_{2g} = b_{3g}$). The excitations from the b_{2g} SOMO to a_u and b_{3u} are translationally allowed ($b_{2g} \times a_u = b_{2u}$ and $b_{2g} \times b_{3u} = b_{1u}$), while the excitation to b_{1g} level is rotationally allowed. The observed rotationally allowed excitations from the highest SOMO levels within the β electron stack can explain why π_β-electron currents are weaker than that of π_α-electrons.

Taken together, with an analysis of the translational and rotational virtual transitions to which the induced current densities can be related, we can achieve an understanding of the strong ring currents in **^{3}B$_4$N$_4$COT-A** and similar azaboraCOTs. These, however, are not necessarily related to the other aspects of triplet state Baird-aromaticity.

4 | CONCLUSIONS

From our computational analysis, it is apparent that borazocine in T_1 (**^{3}B$_4$N$_4$COT-A**) according to energetic and most electronic aromaticity descriptors is as weakly aromatic as borazine in S_0, but when evaluated by magnetic aromaticity indices the first molecule is significantly more aromatic than the latter, as exemplified by NICS $(1)_{zz}$ values of -19.3 and -5.9, respectively. The symmetry properties of the orbitals of borazine in S_0 are such that they provide for both strong translational (diatropic) and rotational (paratropic) transitions. In contrast, for **^{3}B$_4$N$_4$COT-A** the translational transitions are much stronger than the rotational ones, a situation that tends towards that of **^{3}COT** where the rotational transitions are nil. These features lead to significant differences in the extent of aromaticity when evaluated with magnetic as compared to electronic or energetic aromaticity indices.

Our results point to the need to identify further molecules for which the magnetic aspect of aromaticity diverges from the electronic and energetic aspects, similar to what been observed earlier for $(N_6H_6)^{2+}$ and $C_2N_4H_6$.[36] Our findings support the view that one should speak of aromaticity as two phenomena,[36,64] one response aromaticity represented by the magnetic aspect and one intrinsic aromaticity represented by the electronic, energetic and geometric aspects. Our study highlights the importance of considering as many aspects of (Baird-) aromaticity as possible when novel species with potential aromatic characters are evaluated. Besides complications related to the choice of computational method there are also challenges intrinsically related to the electronic structure of the molecules, and both must be incorporated in studies of (excited state) aromaticity and antiaromaticity effects.

ACKNOWLEDGEMENTS

We first thank Ms. Sílvia Escayola Gordils and Prof. Miquel Solà for assistance and feedback on some of the computations. We are grateful to the Wenner-Gren Foundations for a postdoctoral fellowship for P.P. (UPD 2020-0270) and for financial support from the Swedish Research Council (Vetenskapsrådet) (grant 2019-05618). S.R. acknowledges support by the Serbian Ministry of Education, Science and Technological Development (Agreement No. 451-03-68/2022-14/200122). The computations were enabled by resources provided by the Swedish National Infrastructure for Computing (SNIC) at the National Supercomputer Center (NSC), Linköping, Sweden.

ORCID

Nathalie Proos Vedin https://orcid.org/0000-0002-9313-3739
Henrik Ottosson https://orcid.org/0000-0001-8076-1165

REFERENCES

[1] A. Stock, E. Pohland, *Ber. Dtsch. Chem. Ges. A/B* **1926**, *59*, 2215.
[2] D. Benker, T. M. Klapötke, G. Kuhn, J. Li, C. Miller, *Heteroat. Chem.* **2005**, *16*, 311.
[3] D. L. Cooper, S. C. Wright, J. Gerratt, P. A. Hyams, M. Raimondi, *J. Chem. Soc. Perkin Trans.* **1989**, *2*, 719.
[4] I. Neogi, A. M. Szpilman, *Synthesis* **1877**, *2022*, 54.
[5] P. v. R. Schleyer, H. Jiao, N. J. R. E. Hommes, V. G. Malkin, O. L. Malkina, *J. Am. Chem. Soc.* **1997**, *119*, 12669.
[6] P. W. Fowler, E. Steiner, *J. Phys. Chem. A* **1997**, *10*, 1409.
[7] I. D. Madura, T. M. Krygowski, M. K. Cyrański, *Tetrahedron* **1998**, *54*, 14913.
[8] B. Kiran, A. K. Phukan, E. D. Jemmis, *Inorg. Chem.* **2001**, *40*, 3615.
[9] R. Islas, E. Chamorro, J. Robles, T. Heine, J. C. Santos, G. Merino, *Struct. Chem.* **2007**, *18*, 833.
[10] P. F. Fowler, D. E. Bean, M. Seed, *J. Phys. Chem. A* **2010**, *114*, 10742.
[11] R. A. Iwaki, T. Udagawa, *Chem. Phys. Lett.* **2020**, *745*, 137271.
[12] R. Baez-Grez, R. Pino-Rios, *RSC Adv.* **2022**, *12*, 7906.
[13] M. R. Merino-García, L. A. Soriano-Agueda, J. D. Guzmán-Hernández, D. Martínez-Otero, B. Landeros Rivera, F. Cortés-Guzmán, J. E. Barquera-Lozada, V. Jancik, *Inorg. Chem.* **2022**, *61*, 6785.
[14] A. Soncini, C. Domene, J. J. Engelberts, P. W. Fowler, A. Rassat, J. H. van Lenthe, R. W. A. Havenith, L. W. Jenneskens, *Chem.- Eur. J.* **2005**, *11*, 1257.
[15] N. D. Charistos, A. G. Papadopoulos, M. P. Sigalas, *J. Phys. Chem. A* **2014**, *118*, 1113.
[16] N. C. Baird, *J. Am. Chem. Soc.* **1972**, *94*, 4941.
[17] H. Ottosson, *Nat. Chem.* **2012**, *4*, 969.
[18] M. Rosenberg, C. Dahlstrand, K. Kilså, H. Ottosson, *Chem. Rev.* **2014**, *114*, 5379.
[19] J. Kim, J. Oh, A. Osuka, D. Kim, *Chem. Soc. Rev.* **2022**, *51*, 268.
[20] M. Solà, *Nat. Chem.* **2022**, *14*, 585.
[21] L. Karas, J. Wu, *Nat. Chem.* **2022**, *14*, 723.
[22] P. Geymayer, E. G. Rochow, U. Wannagat, *Angew. Chemie Int. Ed.* **1964**, *3*, 633.
[23] W. Storch, W. Jackstiess, P. D. H. Nöth, G. Winter, *Angew. Chem., Int. Ed.* **1977**, *16*, 478.
[24] P. Paetzold, *Phosphorus Sulfur Silicon Relat. Elem.* **1994**, *93*, 39.
[25] Y. Shoji, Y. Ikabata, I. Ryzhii, R. Ayub, O. El Bakouri, T. Sato, Q. Wang, T. Miura, B. S. B. Karunathilaka, Y. Tsuchiya, C. Adachi, H. Ottosson, H. Nakai, T. Ikoma, T. Fukushima, *Angew. Chemie Int. Ed.* **2021**, *60*, 21817.
[26] S. Villaume, H. A. Fogarty, H. Ottosson, *ChemPhysChem* **2008**, *9*, 257.
[27] J. Zhu, C. Dahlstrand, J. R. Smith, S. Villaume, H. Ottosson, *Symmetry* **2010**, *2*, 1653.
[28] S. Taubert, D. Sundholm, J. Juselius, *J. Chem. Phys.* **2011**, *134*, 054123.
[29] P. B. Karadakov, *J. Phys. Chem. A* **2008**, *112*, 12707.
[30] P. B. Karadakov, *J. Phys. Chem. A* **2008**, *112*, 7303.
[31] J. Zhu, K. An, P. R. Schleyer, *Org. Lett.* **2013**, *15*, 2442.
[32] H. S. Turner, R. J. Warne, *Faraday Trans.* **1962**, 69.
[33] P. T. Clarke, H. M. Powell, *J. Chem. Soc. (B)* **1966**, 1172.
[34] C. S. Anstöter, C. M. Gibson, P. W. Fowler, *Phys. Chem. Chem. Phys.* **2020**, *22*, 15919.
[35] M. Monajjemi, *J. Struct. Chem.* **2020**, *61*, 1551.
[36] L. Zhao, R. Grande-Aztatzi, C. Foroutan-Nejad, J. M. Ugalde, G. Frenking, *ChemistrySelect* **2017**, *2*, 863.
[37] P. Lazzaretti, *J. Chem. Phys.* **2018**, *148*, 134109.
[38] M. J. Frisch, G. W. Trucks, H. B. Schlegel, G. E. Scuseria, M. A. Robb, J. R. Cheeseman, G. Scalmani, V. Barone, G. A. Petersson, H. Nakatsuji, X. Li, M. Caricato, A. V. Marenich, J. Bloino, B. G. Janesko, R. Gomperts, B. Mennucci, H. P. Hratchian, J. V. Ortiz, A. F. Izmaylov, J. L. Sonnenberg, D. Williams-Young, F. Ding, F. Lipparini, F. Egidi, J. Goings, B. Peng, A. Petrone, T. Henderson, D. Ranasinghe, V. G. Zakrzewski, J. Gao, N. Rega, G. Zheng, W. Liang, M. Hada, M. Ehara, K. Toyota, R. Fukuda, J. Hasegawa, M. Ishida, T. Nakajima, Y. Honda, O. Kitao, H. Nakai, T. Vreven, K. Throssell, J. A. Montgomery, Jr., J. E. Peralta, F. Ogliaro, M. J. Bearpark, J. J. Heyd, E. N. Brothers, K. N. Kudin, V. N. Staroverov, T. A. Keith, R. Kobayashi, J. Normand, K. Raghavachari, A. P. Rendell, J. C. Burant, S. S. Iyengar, J. Tomasi, M. Cossi, J. M. Millam, M. Klene, C. Adamo, R. Cammi, J. W. Ochterski, R. L. Martin, K. Morokuma, O. Farkas, J. B. Foresman, D. J. Fox, Gaussian, Inc., Wallingford CT, **2016**.
[39] A. D. Becke, *Phys. Rev. a* **1988**, *38*, 3098.
[40] C. Lee, W. Yang, R. G. Parr, *Phys. Rev. B* **1988**, *37*, 785.
[41] N. C. Handy, A. Cohen, *Mol. Phys.* **2001**, *99*, 403.
[42] A. D. Becke, *J. Chem. Phys.* **1993**, *98*, 5648.
[43] P. J. Stephens, F. J. Devlin, M. J. Frisch, C. F. Chabalowski, *J. Phys. Chem.* **1994**, *98*, 11623.
[44] T. Yanai, D. Tew, N. Handy, *Chem. Phys. Lett.* **2004**, *393*, 51.
[45] J.-D. Chai, M. Head-Gordon, *Phys. Chem. Chem. Phys.* **2008**, *10*, 6615.
[46] R. Krishnan, J. S. Binkley, R. Seeger, J. A. Pople, *J. Chem. Phys.* **1980**, *72*, 650.
[47] D. W. Szczepanik, M. Andrzejak, K. Dyduch, E. Żak, M. Makowski, G. Mazur, J. Mrozek, *Phys. Chem. Chem. Phys.* **2014**, *16*, 20514.
[48] D. W. Szczepanik, M. Andrzejak, J. Dominikowska, B. Pawełek, T. M. Krygowski, H. Szatylowicz, M. Solà, *Phys. Chem. Chem. Phys.* **2017**, *19*, 28970.
[49] P. V. R. Schleyer, C. Maerker, A. Dransfeld, H. Jiao, N. J. R. van Eikema Hommes, *J. Am. Chem. Soc.* **1996**, *118*, 6317.
[50] Z. Chen, C. S. Wannere, C. Corminboeuf, R. Puchta, P. v. R. Schleyer, *Chem. Rev.* **2005**, *105*, 3842.
[51] D. Geuenich, K. Hess, F. Köhler, R. Herges, *Chem. Rev.* **2005**, *105*, 3758.
[52] M. Giambiagi, M. Segre de Giambiagi, C. D. dos Santos Silva, A. Paiva de Figueiredo, *Phys. Chem.Chem. Phys.* **2000**, *2*, 3381.
[53] P. Bultinck, R. Ponec, S. Van Damme, *J. Phys. Org. Chem.* **2005**, *18*, 706.
[54] E. Matito, M. Duran, M. Solà, *J. Chem. Phys.* **2005**, *122*, 014109.
[55] M. Krygowski, H. Szatylowicz, O. A. Stasyuk, J. Dominikowska, M. Palusiak, *Chem. Rev.* **2014**, *114*, 6383.

[56] P. v. R. Schleyer, F. Puhlhofer, *Org. Lett.* **2002**, *4*, 2873.
[57] T. A. Keith, R. F. W. Bader, *J. Chem. Phys.* **1993**, *99*, 3669.
[58] P. Lazzeretti, M. Malagoli, R. Zanasi, *Chem. Phys. Lett.* **1994**, *220*, 299.
[59] T. A. Keith, R. F. W. Bader, *Chem. Phys. Lett.* **1993**, *210*, 223.
[60] S. Coriani, P. Lazzeretti, M. Malagoli, R. Zanasi, *Theor. Chim. Acta* **1994**, *89*, 181.
[61] T. Franz, E. Hanecker, H. Nöth, W. Stöcker, W. Storch, G. Winter, *Chem. Ber.* **1986**, *119*, 900.
[62] A. Rehaman, A. Datta, S. S. Mallajosyula, S. K. Pati, *J. Chem. Theory Comput.* **2006**, *2*, 30.
[63] Y. C. Lin, D. Sundholm, J. Jusélius, *J. Chem. Theory Comput.* **2006**, *2*, 761.
[64] T. Janda, C. Foroutan-Nejad, *ChemPhysChem* **2018**, *19*, 2357.
[65] O. W. David, R. Christopher, *Adv. Heterocycl. Chem.* **1976**, *19*, 1.
[66] W. Baker, W. D. Ollis, Q. Rev, *Chem. Soc.* **1957**, *11*, 15.
[67] B. V. Badami, *Resonance* **2006**, *11*, 40.
[68] M. Baranac-Stojanović, *Chem. – Eur. J.* **2014**, *20*, 16558.
[69] E. Steiner, P. W. Fowler, *J. Phys. Chem. A* **2001**, *105*, 9553.

SUPPORTING INFORMATION

Additional supporting information can be found online in the Supporting Information section at the end of this article.

How to cite this article: P. Preethalayam, N. Proos Vedin, S. Radenković, H. Ottosson, *J Phys Org Chem* **2023**, *36*(1), e4455. https://doi.org/10.1002/poc.4455